Journal of Engineering, Project, and Production Management
2026, 16(5), 2025-253

Time-Series Prediction of Scenic Area Climate Suitability via DTW-LSTM Model and Tourism Development Correlation

Xiaojing Liu
Lecturer, Business School, Xuchang University, Xuchang 461000, China, E-mail: xcuxiaoyue1115@163.com

Project Management
Received November 3, 2025; revised December 21, 2025; accepted March 9, 2026
Available online June 17, 2026

Abstract: Traditional methods face two key limitations. First, they cannot effectively capture complex nonlinear fluctuations driven by tourist's perception patterns in the climate sequence, which undermines predictive accuracy. Second, few studies have systematically and dynamically linked high-precision climate predictions with multi-dimensional tourism development indicators. To this end, the research applies the dynamic time regularization algorithm to capture the climate fluctuation patterns of "similar days" that conform to tourist's subjective perceptions and constructs a dual-branch Long Short-Term Memory (LSTM) network to improve the modeling accuracy of complex nonlinear dynamics of climate suitability. Moreover, the grey relational analysis method is adopted to conduct correlation analysis. Results indicated that the proposed model demonstrated outstanding performance in climate suitability prediction. Its mean absolute error was 0.92, root mean squared error was 1.35, mean absolute percentage error was 2.84%, and coefficient of determination reached 0.94, significantly outperforming traditional and single models. Correlation analysis indicated that between 2010 and 2020, the correlation coefficient between the comprehensive comfort index and annual visitor numbers steadily increased from 0.68 to 0.83. This demonstrated that comfortable climate conditions have become a key factor influencing tourists' travel decisions. The model proposed by the research enhances the predictive accuracy of climate suitability in scenic areas and reveals a progressively stronger correlation between climate comfort and tourist flow volume. This provides precise data support and decision-making basis for scenic areas to address climate change and optimize visitor flow management.

Keywords: Climate suitability, grey relational analysis; LSTM neural network, tourism demand analysis, time-series forecasting.

DOI 10.32738/JEPPM-2025-253

1. Introduction

Global climate change and the growing tourism industry significantly influence the sustainability of regional tourism economies. Climate change has caused more frequent extreme weather events and shifts in seasonal patterns, directly affecting the environmental comfort and natural resources of tourist destinations (Gong et al., 2024). As a climate-sensitive industry, tourism relies heavily on climate factors such as temperature, humidity, sunshine duration, and wind speed to inform traveler's decisions and the quality of their experience. Therefore, predicting the climatic suitability of scenic areas and analyzing their relationship with tourism activities has become a crucial practical need (Lopes et al., 2024; Quibus et al., 2022). Traditional statistical Time Series (TS) forecasting methods handle linear problems well. However, when faced with the complex, nonlinear, nonstationary, and seasonal nature of climate data, their accuracy and generalization often fall short (Cao et al., 2023). Deep Learning (DL) methods, especially LSTM networks, have advanced significantly in recent years for various TS forecasting tasks because of their ability to recognize sequential patterns and Long-Range Dependencies (LRDs). Nevertheless, when managing climate sequences with complex fluctuations, a single LSTM model may sometimes miss internal dynamic shape similarities, leading to lag or biases in predicting critical inflection points (Sato and Fujimoto 2024). The Dynamic Time Warping (DTW) algorithm is an effective tool for measuring TS similarity. It effectively addresses stretching and distortion along the time axis and can accurately identify "similar days" in historical data that display patterns akin to the current forecast period (Filipovska and Mahmassani 2023; Ridderstaat 2023).

Climate suitability, a key environmental factor shaping tourist travel decisions and experience quality, has become a focal point in tourism geography research due to the need for accurate prediction and understanding of its links to tourism activities. To address the challenge of modeling the relationships between weather conditions and both short- and long-range spatial dependencies in multi-meteorological forecasting, Xu et al. (2024) proposed a tensor-based convolutional model for both short- and long-term predictions. This model identified the contributions from different grid points and weather conditions to forecasts using node and relationship attention mechanisms, while applying adaptive tensor graph convolutions to capture long-range dependencies. Results showed significantly improved predictive performance compared to existing methods. To improve the forecasting accuracy of direct normal irradiance. Pereira et al. (2024) developed a prediction model based on artificial neural networks. They designed two neural network architectures: one that directly uses meteorological variables at the forecast time, and another that incorporates forecast sequences to enhance predictive accuracy. Experiments revealed that this model outperformed traditional numerical weather prediction outputs. To enhance high-precision temperature forecasting, Gogen and Guney (2024) used upper-air radiosonde data to predict the next day's maximum and minimum temperatures (MaxT and MinT) with machine learning algorithms. After comparing multiple regression methods, the Gaussian process regression showed the best results. Han et al. (2023) created a multi-view, multi-adversarial learning framework to better utilize the natural correlations in weather and air quality forecasting tasks. This approach employed evolutionary recurrent networks to capture dynamic temporal dependencies and used multi-adversarial mechanisms to reduce observational noise. Experiments confirmed that the model effectively integrated air quality and meteorological data. To address the challenge of simultaneously capturing local and global spatio-temporal dependencies in weather forecasting, Zhang and Zhou (2025) developed a dual-branch architecture combining convolutional LSTMs and transformers to extract local features and global context, respectively, while incorporating a partial differential equation module. Tests across multiple meteorological datasets showed that this model outperformed existing advanced methods in both prediction accuracy and computational efficiency.

To improve the accuracy of daily visitor flow forecasting in scenic areas, Li (2024) suggested including Baidu Index as an external feature in the LSTM prediction model. The study examined the relationships among nine features, such as date type, holidays, weather, and past visitor numbers, and conducted experiments at Longkou Nanshan Scenic Area. Results showed that LSTM predictions outperformed Support Vector Machines (SVMs) and backpropagation neural networks. To enhance tourism service quality in the 5G multimedia environment, Yan et al. (2024) proposed a deep learning-based fusion model that combines convolutional neural networks with LSTM for analyzing user review sentiment and providing personalized recommendations. Experiments revealed that this model outperformed SVMs, Random Forests (RF), and single LSTM models. Given the highly nonlinear and constantly changing nature of hydrological TS, Huang et al. (2023) suggested an encoder-decoder LSTM model with spatiotemporal attention mechanisms for predicting hydrological data collected by wireless sensors. This model showed strong generalization abilities by adaptively capturing key features through spatial attention and focusing on crucial time steps via temporal attention. To explore dynamic clustering patterns in international hotel tourism demand, Ruiz Reina (2025) used the DTW method to align and cluster 106 international demand TS. This approach automatically found the best number of clusters and identified common patterns and outliers. Results indicated that the method effectively captured the effects of events. To address the coarse detail in existing tourism seasonality analysis and the difficulty in detecting subtle changes, Wang et al. (2023) introduced a recognition and forecasting method using DTW and density peak clustering. This technique identified tourism seasonal patterns from daily data, matched patterns, and then forecasted demand. Results showed that this method accurately captured intraday and interday seasonal trends, detected subtle shifts, such as off-peak travel, and significantly improved forecasting accuracy. In summary, traditional models struggle to capture medium- to long-term dependencies and complex nonlinear relationships within TS data. Machine learning models inadequately account for the interdependence within TS data, and a single LSTM model shows significant prediction errors during periods of high data volatility. In tourism suitability research, most studies focus solely on climate dimensions while overlooking other influencing factors such as scenic area information and tourist flow. Moreover, these studies are often limited to past evaluations, lacking predictions for future suitability trends and thus failing to offer comprehensive guidance for tourists and the industry. Therefore, this study proposes a framework combining DTW and LSTM for TS forecasting and correlation analysis. The method innovatively uses the DTW algorithm to perform elastic alignment and shape matching on historical climate TS, identifying "similar days" with highly comparable fluctuation patterns to the forecast period. This captures tourist's subjective perception patterns of climatic conditions. Next, a dual-branch LSTM network is built to learn the dynamic variation patterns of climate suitability from both the overall TS and similar local segments. Building on this, the study further integrates climate comfort analysis with grey relational analysis to quantify the dynamic correlation strength between climate suitability and various aspects of tourism development indicators.

The innovations of this paper are as follows: (1) A dynamic alignment and dual branch learning framework oriented to the complex climate tourism system of scenic spots is proposed: the DTW algorithm is innovatively used to identify historical "similar days" with similar tourist perception fluctuation patterns in the prediction period, not only for similarity measurement, so as to introduce human subjective perception of climate into the prediction model. (2) Realize the dynamic correlation quantification between climate suitability prediction and multi-dimensional tourism development: beyond single climate prediction or static correlation analysis, through gray correlation analysis, dynamically quantify the correlation strength and time sequence evolution between climate comfort and multiple indicators such as tourist volume and tourism income. (3) Provide transferable methodology and case verification: Huangshan Scenic Area is taken as a typical case for verification, but the model design considers universality, and its framework can be adapted to other

mountain types and natural landscape tourist attractions, providing a method reference for adaptive management of different tourism environments.

2. Methods

This study employs a fusion modeling approach combining DTW and LSTM. DTW is utilized to perform elastic alignment and same-day screening of climate TS data. Subsequently, a dual-branch LSTM network is constructed to learn global trends and local fluctuation characteristics, respectively. Finally, predictions are generated through adaptive weighted fusion. Concurrently, gray relational analysis is applied to quantitatively evaluate the dynamic correlation between climate suitability and tourism development.

2.1. Construction of the DTW-LSTM Fusion Model

Research on the correlation between TS forecasting of scenic area climate suitability and tourism development essentially represents an in-depth exploration of environmental perception and behavioral response mechanisms within human-land interactions. Climate conditions not only directly shape the resource attractiveness of tourist destinations but also indirectly regulate the spatiotemporal distribution of tourist flows and the quality of visitor experiences by influencing traveler's perceived comfort levels and psychological expectations (Sierra-Porta, 2025). Traditional research often relies on static cross-sectional data or simple meteorological indicators, making it difficult to capture the dynamic adaptation process of tourism demand under climate change. Introducing TS forecasting methods enables analysis of the coupling between historical climate patterns and tourism behavior, thereby revealing the underlying dynamic mechanisms of their correlation. Precise climate suitability forecasts provide scientific travel guides for tourists, particularly enhancing travel safety and equitable experiences for climate-sensitive groups such as the elderly and children. Simultaneously, they offer decision support to scenic area managers for optimizing resource allocation and mitigating climate risks, thereby advancing sustainable development and adaptive governance in tourism amid climate change.

In the design of the DTW-LSTM model, the first challenge is addressing the similar measurement of climate TS data. Climate data (such as daily MaxT, relative humidity, wind speed, etc.) often exhibit non-uniform lengths due to issues such as temporary equipment failures or data transmission delays. Furthermore, climate sequences from the same period across different years may suffer from time-axis scaling. Traditional Euclidean distance struggles to accurately measure the similarity of such sequences (Sabarinath et al., 2023; Alhindi et al., 2025). To achieve effective similarity measurement for climate TS data, this study implements elastic alignment through a three-step process: Distance Matrix (DM) construction, loss matrix calculation, and regularized path optimization. This process is illustrated in Fig. 1.

	2	6	7	5	6	7	2	1
3	1	3	4	2	3	4	1	2
6	4	0	1	1	0	1	4	5
8	6	2	1	3	2	4	6	7
5	3	1	2	0	1	2	3	4
7	5	1	0	2	1	0	5	6
2	0	4	5	3	4	5	0	1

(a) Distance matrix D

	2	6	7	5	6	7	2	1
3	1	1+3=4	8	10	13	17	18	20
6	1+4-5	1+0-1	5	3	3	4	8	13
8	11	3	5	5	5	4	10	15
5	14	4	4	2	3	5	7	11
7	19	5	4	4	3	3	8	13
2	19	9	9	7	7	8	3	4

MIN

(b) Loss matrix D_c

Fig. 1. Schematic diagram of the distance matrix and cumulative loss matrix calculation in the DTW algorithm

It is assumed that two series of scenic area climate suitability exist, designated as the reference series $X=(x_1,x_2,...,x_m)$ and test series $Y=(y_1,y_2,...,y_n)$. First, the DM D is constructed for $m\times n$. Matrix element $D(i,j)$ represents the local difference between the i th element of series X and the j th element of series DD. Euclidean distance is employed to quantify the correlation between data points at a single time step, as shown in Eq. (1).

$$D(i,j)=\left|x_i-y_j\right|^2 \tag{1}$$

Fig. 1(a) illustrates the specific structure of this DM. The different values within the matrix directly reflect the local differences in climate suitability between the two sequences at each point in time. For example, the value D(8,7) corresponding to November 8 (i=8) and November 7 (j=7) is relatively low, indicating that the climate suitability states of the two sequences are similar at that point in time.

Based on dynamic programming principles, the loss matrix D_c is further computed to achieve elastic sequence alignment, with the calculation process subject to three constraints. First, the boundary constraint requires alignment paths to originate from $D_c(1,1)$ and terminate at $D_c(m,n)$, ensuring complete matching at the sequence's beginning and end. Second, the monotonicity requirement stipulates that paths extend only in the right, down, and right-down directions to

prevent temporal sequence disruption. Finally, the continuity requirement mandates path continuity without jumps to guarantee alignment smoothness. The loss matrix is updated recursively by combining the minimum loss value of adjacent positions with the current local distance (Singh et al., 2025; Li et al., 2025), as shown in Eq. (2).

$$D_c(i,j) = \min\left\{D_c(i-1,j-1), D_c(i-1,j), D_c(i,j-1)\right\} + D(i,j) \tag{2}$$

In Eq. (2), the initial value $D_c(1,1) = D(1,1)$ is computed by traversing the matrix element-by-element. The $D_c(m,n)$ value in the lower-right corner of the final matrix represents the DTW distance between the two sequences. Sequence patterns are more similar when the value is smaller (Cao et al., 2024). Fig. 1(b) presents the computed loss matrix. The values in the lower-right corner can be directly used to assess the overall similarity between climate suitability sequences for the same period across different years. To determine the specific alignment relationship between two sequences, an optimal matching pair must be identified through path regularization optimization. The results of this process are shown in Fig. 2.

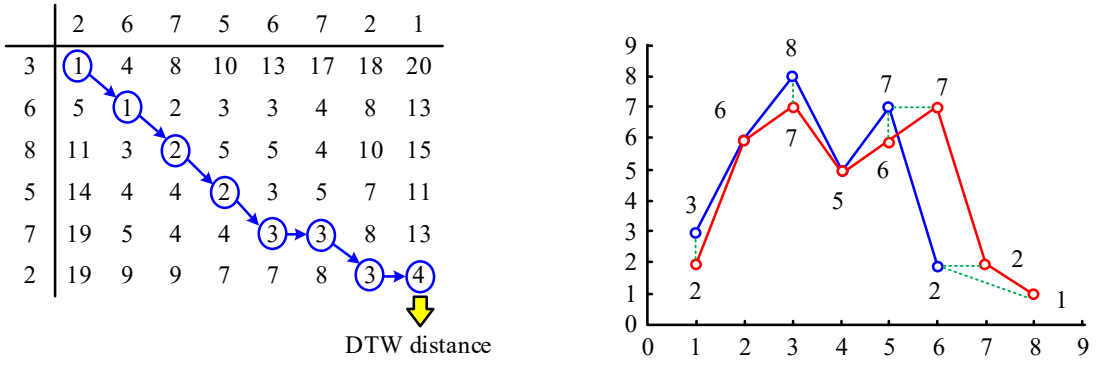

(a) Standardize the path and DTW distance (b) Alignment of points

Fig. 2. Optimal path and sequence alignment matching results based on DTW

Fig. 2(a) shows the optimal regular path, indicated by the solid line from the top-left to the bottom-right corner. Each node (i,j) along the path corresponds to the optimal matching relationship between the i th element of sequence X and the j th element of sequence Y. Fig. 2(b) further visualizes the matching logic. For example, when sequence Y has missing data on November 5th, the path can be extended to align November 5th in sequence X with November 4th in sequence Y, effectively resolving the challenge of matching sequences of unequal lengths. In climate data processing, a 1×7 weekly time window can be configured to traverse historical climate data. Using sequences with climate suitability within the suitable range as reference templates, the DTW distance between each test template and the reference template is calculated. Those with distances below the threshold are selected. That is, dates corresponding to test templates with similarity exceeding the set standard are designated as "similar days," providing high-quality sample support for subsequent LSTM training.

To address the LRD characteristics of climate suitability changes, this study employs an LSTM network to circumvent the vanishing gradient problem inherent in traditional recurrent neural networks. The core mechanism achieves temporal screening and retention by coordinating the Forget Gate (FG), Input Gate (IG), and Output Gate (OG). Specifically, the FG filters effective information from historical Cell States (CSs), determining whether to retain or discard past temporal features, as illustrated in Eq. (3).

$$f_t = \sigma\left(W_f \cdot [h_{t-1}, x_t] + b_f\right) \tag{3}$$

In Eq. (3), W_f and b_f display the weight parameter and bias term of the forgetting gate. h_{t-1} denotes the network's hidden-layer output at the previous step. x_t represents the climate feature data input at the current time step. σ is the sigmoid Activation Function (AF) (output range [0,1]). In climate data processing, the forgetting gate automatically filters out irrelevant short-term information, such as minor daily wind speed fluctuations, while prioritizing the retention of key long-term features, such as monthly temperature trends (Shang et al., 2025). The IG updates CSs to determine new temporal information to incorporate at the current time step, comprising two steps: candidate state generation and state update, as shown in Eq. (4).

$$\begin{cases} i_t = \sigma\left(W_i \cdot [h_{t-1}, x_t] + b_i\right) \\ \tilde{C}_t = \tanh\left(W_C \cdot [h_{t-1}, x_t] + b_C\right) \\ C_t = f_t \cdot C_{t-1} + i_t \cdot \tilde{C}_t \end{cases} \tag{4}$$

In Eq. (4), i_t represents the IG activation value. $\tilde{C}_t$ denotes the candidate CS (the tanh AF ensures output ranges from -1 to 1). C_t indicates the updated CS. This process accurately captures abrupt changes in climate data, such as the sudden increase in humidity 2-3 days before a typhoon arrives and incorporates these critical features into the CS via the IG (Li et al., 2024). The OG controls the informational content of the hidden layer's current output, filtering features within the CS that are strongly correlated with future climate suitability, as shown in Eq. (5).

$$\begin{cases} o_t = \sigma\left(W_o \cdot [h_{t-1}, x_t] + b_o\right) \\ h_t = o_t \cdot \tanh(C_t) \end{cases} \tag{5}$$

In Eq. (5), o_t represents the OG activation value. h_t denotes the hidden layer output at the current time step. For climate suitability forecasting, the OG can prioritize core features such as temperature variations and humidity trends over the next three days, enhancing the prediction's relevance and effectiveness. The final DTW-LSTM fusion model workflow is illustrated in Fig. 3.

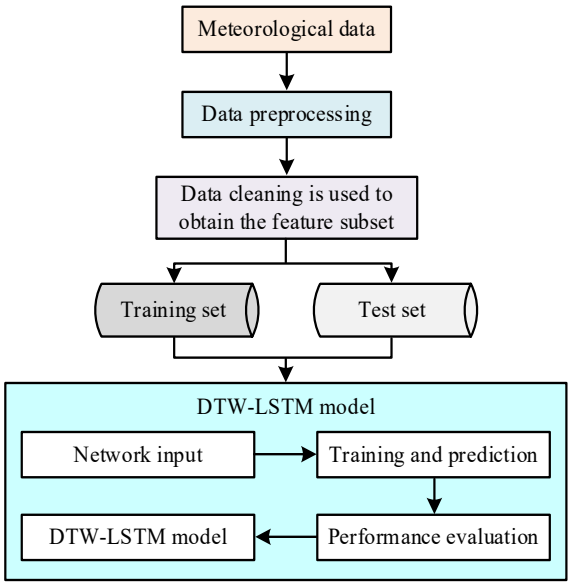

Fig. 3. The process of the DTW-LSTM fusion model

In the model training phase of Fig. 3, a dual LSTM network is employed for parallel training to achieve multi-perspective learning of data features. The complete original training set (denoted as Train_DATA) and the augmented training set obtained through DTW filtering (denoted as DTW_DATA) are respectively input into two structurally identical LSTM models. The LSTM model trained on Train_DATA focuses on learning long-term trends in global temporal data, while the LSTM model trained on DTW_DATA concentrates on capturing local fluctuation patterns within similar periodic segments. Network weights are updated during training using the Adam optimizer, which allocates adaptive learning rates to each parameter according to first- and second-order moment estimations. Early stopping is employed to reduce overfitting probability, ensuring both sub-models converge stably and learn effective features.

Finally, the prediction results from the dual models are integrated through weighted fusion. The weight calculation is primarily based on the DTW similarity metric, ensuring that model predictions dominated by similar data carry greater influence. The weight calculation for the LSTM model based on DTW_DATA is shown in Eq. (6).

$$w = \frac{minDTW(X_i, Y)}{\sum_{1}^{k} DTW(X_i, Y) + DTW(N, Y)} \tag{6}$$

In Eq. (6), $minDTW(X_i, Y)$ represents the minimum DTW distance between the selected k data sets and the reference sequence (RS) Y. $\sum_{1}^{k} DTW(X_i, Y)$ denotes the sum of DTW distances between k data sets and Y. $DTW(N, Y)$ signifies the DTW distance between the original training set and Y. The final prediction result $\hat{y}_t$ is obtained by weighting the predictions $\hat{y}_{\text{LSTM}}$ and $\hat{y}_{\text{DTW-LSTM}}$ from the two LSTM models, as shown in Eq. (7).

$$\hat{y}_t = (1 - \lambda) \cdot \hat{y}_{\text{LSTM}} + \lambda \cdot \hat{y}_{\text{DTW-LSTM}} \tag{7}$$

In Eq. (7), λ represents the dynamic weight, which is adaptively adjusted based on DTW similarity and the model's

performance on the validation set. This fusion approach preserves the influence of global temporal trends and enhances the contribution of similar periodic segments to prediction outcomes. This effectively improves the model's ability to adapt to highly volatile TS data.

2.2. Correlation Analysis Between Tourism Development and Climate Suitability

Building upon the precise climate suitability predictions achieved by the DTW-LSTM fusion model for scenic areas, this study further employs grey relational analysis to systematically quantify the dynamic correlation strength between climate suitability and multiple tourism development indicators. This approach aims to reveal the intrinsic connection between climatic conditions and tourism development, thereby providing a scientific basis for scenic areas to respond to climate change and optimize tourism management strategies. Climate suitability not only directly determines visitors' perceived comfort levels but also indirectly influences the attractiveness of tourism resources, the feasibility of tourism activities, and the overall competitiveness of tourism destinations (Malinović-Milićević et al., 2025). Fig. 4 illustrates the fundamental mechanism by which climate change impacts the tourism industry. The influence of climate suitability on tourism can be analyzed from both direct and indirect dimensions. Direct impacts manifest in aspects such as tourists' travel decisions, length of stay, activity choices, and satisfaction levels. Multiple studies indicate that extreme weather events significantly reduce tourists' willingness to travel, potentially leading to trip interruptions or cancellations. Indirect impacts manifest in the long-term effects of climate suitability on tourism resources, infrastructure, and service systems. For instance, prolonged heatwaves may cause degradation of the natural landscape, affecting the sustainable use of ecotourism resources. Extreme precipitation events can trigger disasters such as floods and landslides, damaging tourism transportation networks and facility safety, thereby further constraining the healthy development of the tourism industry.

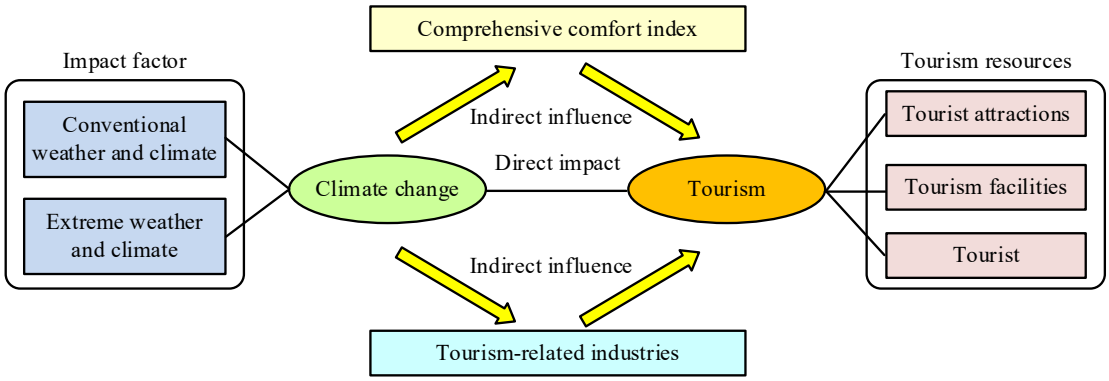

Fig. 4. Schematic diagram of the basic mechanism by which climate change affects the tourism industry

Climate suitability serves as a key driver, directly impacting the tourism industry, such as through policy restrictions affecting tourism operations, while simultaneously exacerbating or alleviating environmental issues. Both typical weather and climate trends, as well as extreme weather and climate events, have an impact on climate change itself. These factors exert indirect effects on tourism-related industries. Quantifying climate suitability typically relies on a comprehensive assessment of multiple meteorological elements. Common Comprehensive Comfort Indices (CCI) include the Temperature-Humidity Index (THI), Wind Chill Index (WCI), and Index of Clothing (ICL). These indices integrate meteorological factors such as temperature, humidity, wind speed, and solar radiation to reflect human thermal comfort perceptions under specific environmental conditions (Gebrehiwot et al., 2024; Kovács et al., 2025). CCI can be expressed as Eq. (8).

$$\mathrm{CCI} = 0.6 \cdot X_{\mathrm{THI}} + 0.3 \cdot X_{\mathrm{WCI}} + 0.1 \cdot X_{\mathrm{ICL}} \tag{8}$$

In Eq. (8), X_{THI}, X_{WCI}, and X_{ICL} represent the normalized values of THI, WCL, and ICL, respectively. This model fully accounts for the varying contributions of different meteorological elements to human comfort, providing a unified metric for climate suitability that facilitates subsequent correlation analyses.

The core of static correlation analysis lies in quantifying the strength of association between climate suitability and tourism development indicators. Among these methods, grey correlation analysis has emerged as a key approach for adapting to the characteristics of meteorological and tourism data due to its advantages: low sample size requirements, no need for data to follow a normal distribution, and effective handling of incomplete information systems (Basegmez et al., 2025). This method reveals the degree of correlation between the reference series (tourism development indicators) and the comparison series (climate indicators) by calculating their association. The reference series comprises core indicators reflecting tourism development levels, including domestic tourist arrivals Y_1, international tourist arrivals Y_2, and total tourism revenue Y_3. These indicators directly reflect the operational status of the tourism industry. The comparison sequences (CSeq) are divided into two categories: First, single meteorological factor sequences, such as annual average temperature (X_1), annual average humidity (X_2), annual average precipitation (X_3), annual average wind speed (X_4), and annual average sunshine duration (X_5). Second is a comprehensive multi-meteorological factor sequence, namely the

composite CCL X_{CCI}. By comparing these two types of sequences, the differences in the impact of single versus multiple factors on tourism development can be distinguished.

First, normalization of the data is performed, as meteorological and tourism data exhibit significant differences in magnitude and units. Direct calculations would distort correlation results. Therefore, dimensionless processing is required to convert all sequences into standardized data within the [0,1] range. Common methods include the mean method and the initial value method, with selection based on data characteristics. The mean method is suitable for sequences with high volatility and no obvious linear trends, such as precipitation and wind speed, as shown in Eq. (9).

$$x_{ik} = \frac{x_i(k)}{\frac{1}{m}\sum_{k=1}^{m} x_i(k)} \tag{9}$$

In Eq. (9), $x_i(k)$ means the raw data of the i-th sequence (e.g., annual average precipitation) at time k. m denotes the number of observations. x_{ik} indicates the standardized data. This method eliminates differences in magnitude by dividing by the sequence mean while preserving the relative fluctuation characteristics of the data. The initial value method is applicable to sequences exhibiting pronounced growth or decline trends, such as passenger volume and tourism revenue, as shown in Eq. (10).

$$x_{ik} = \frac{x_i(k)}{x_i(1)} \tag{10}$$

In Eq. (10), $x_i(1)$ represents the initial-time data of the i-th sequence. By comparing this value with the initial value, the long-term trend of the sequence is highlighted. The correlation difference sequence measures the local deviation between the RS and the CSeq at each time interval. For time k, the correlation difference formula between the RS $Y_0(k)$ and the i-th CSeq $X_i(k)$ is given by Eq. (11).

$$\Delta_i(k) = \left| Y_0(k) - X_i(k) \right| \tag{11}$$

In Eq. (11), $\Delta_i(k)$ means the absolute difference between the i-th CSeq and the RS at time point k. By calculating $\Delta_i(k)$ for all time points, the correlation difference sequence between the CSeq and the RS is obtained. A smaller difference indicates that the two sequences exhibit a more similar trend of change at that time point. Then, traverse all CSeqs and their corresponding association differences at every time point, selecting the global minimum and maximum values. This standardizes the measurement scale for association differences across different sequences, preventing bias in association coefficients caused by sequence variation (Liu et al., 2024). The association coefficient quantifies the closeness of association between the RS and the CSeq at a given time point, as shown in Eq. (12).

$$\xi_i(k) = \frac{\max\limits_{i,k}\Delta_i(k) + \rho \cdot \max\limits_{i,k}\Delta_i(k)}{\Delta_i(k) + \rho \cdot \max\limits_{i,k}\Delta_i(k)} \tag{12}$$

In Eq. (12), $\xi_i(k) \in [0,1]$ represents the correlation coefficient between the i-th CSeq and the RS at time k. If $\xi_i(k)$ approaches 1, it indicates a strong correlation between the two at that time. A weak association is shown if it gets close to 0. ρ is the discrimination coefficient, typically set to 0.5. Its function is to balance the sensitivity and stability of the correlation coefficient. A smaller ρ value indicates more pronounced differences in correlation coefficients and higher sensitivity. A larger ρ value results in smoother correlation coefficients and greater stability. While the correlation coefficient reflects the degree of association at a specific moment, the correlation degree provides a comprehensive measure of the overall association strength across the entire time period. It is obtained by averaging the correlation coefficients for all time points of a given CSeq, as shown in Eq. (13).

$$r_i = \frac{1}{m}\sum_{k=1}^{m} \xi_i(k) \tag{13}$$

In the Eq. (13), $r_i \in [0,1]$ displays the correlation between the i-th CSeq and the RS. A higher correlation indicates a stronger long-term association between the two.

3. Results and analysis

Based on daily-scale meteorological and tourist flow data from Huangshan Scenic Area between 2010 and 2020, this study first verifies the superiority of the DTW-LSTM fusion model in predicting climate suitability. Subsequently, through grey correlation and correlation analysis, it reveals a significantly enhanced dynamic relationship between CCI and tourist flow.

3.1. DTW-LSTM Fusion Model Prediction Results and Accuracy Validation

The datasets used by the research primarily originate from two authoritative departments: First, the daily meteorological data for Huangshan Scenic Area (including but not limited to key indicators such as daily maximum/MinTs, relative humidity, precipitation, sunshine duration, and wind speed) is sourced from the National Meteorological Science Data Center of the China Meteorological Data Network (http://data.cma.cn/). Long-term historical observation data from meteorological monitoring stations surrounding the specific scenic area are obtained through a formal application. Second, the corresponding daily visitor flow data for the scenic area is compiled through the official annual statistical reports of the Huangshan Scenic Area Management Committee, data interfaces from the smart tourism platform, or internally obtained data through collaborative partnerships. To ensure the consistency of TS data, the study selects a complete ten-year dataset of daily data from 2010 to 2020 as the sample. After data cleaning and outlier handling, the meteorological data is utilized to construct a climate suitability index. This index is then aligned with tourism flow data to fully support the subsequent training of the DTW-LSTM fusion model and correlation analysis.

The study employs a time-based partitioning strategy, dividing the daily data from 2010 to 2020 into training, validation, and test sets in a 7:2:1 ratio to simulate real-world forecasting scenarios and prevent information leakage. The experiment is completed on an Ubuntu 20.04 server configured with Python 3.8, TensorFlow 2.8.0 with Keras 2.8.0, NVIDIA GeForce RTX 3080, and NVIDIA Driver version 510.54 to ensure reproducibility of results. Table 1 displays the DTW-LSTM fusion model's parameters.

Table 1. Parameter settings of the DTW-LSTM fusion model

Block	Parameter	Values/settings
LSTM structure	Number of network layers	2
	Number of hidden units	64
	Enter the time step	14
	Output the time step	7
	Dropout	0.2
Training settings	Optimizer	Adam
	Learning rate	0.001
	Batch size	32
	Epochs	200
	Patience	20

Table 2 demonstrates the prediction performance of the DTW-LSTM model for the TS data of scenic area climate suitability. By comparing the Actual Values (AVs) and Predicted Values (PVs) over consecutive days in late December 2018, it is evident that the model exhibits a low overall prediction error, with the absolute error falling below 1 for the vast majority of dates. This indicates that the model possesses a certain degree of capability in predicting climate suitability. However, relatively high errors (approaching 0.9) are observed on dates such as December 23, 27, and 30, indicating that the model's stability during specific weather shifts or complex meteorological conditions still has room for improvement. This underscores the necessity of introducing the DTW-LSTM hybrid model for TS alignment and nonlinear dynamic modeling. The fluctuating aspects of climate appropriateness and their possible influence on tourism activities are better captured by this model.

Table 2. DTW-LSTM predicted versus true value comparison results

Date	Actual value	Predicted value	Error value
2018/12/20	35.12	35.65	-0.53
2018/12/21	38.75	38.98	-0.23
2018/12/22	44.08	44.29	-0.21
2018/12/23	36.26	35.35	0.91
2018/12/24	38.63	39.31	-0.68
2018/12/25	40.47	41.32	-0.85
2018/12/26	36.84	36.31	0.53
2018/12/27	44.16	43.27	0.89
2018/12/28	41.72	42.11	-0.39

2018/12/29	34.18	33.82	0.36
2018/12/30	31.76	30.85	0.91

The comparison of late December 2018 temperature estimates and actual results for various models is displayed in Fig. 5. In Fig. 5(a), the CNN model's prediction curve exhibits poor alignment with AVs, with significant deviations observed on certain dates. For instance, the PV on December 20 is 1.5 degrees lower than the AV, while the PV on December 26 is 1.8 degrees higher than the AV. The overall error range falls between 1.2 and 1.8 degrees. Fig. 5(b) shows that the LSTM model outperforms the CNN in prediction accuracy, reducing the error to 0.8-1.3. The PV on December 24 is 1.1 higher than the AV, while the PV on December 28 is 0.8 lower than the AV, though visible deviations still exist. In Fig. 5(c), the DTW-LSTM model's prediction curve closely aligns with the AVs, with errors ranging from 0.2 to 0.5. The difference between the PV and AV is 0.3 on December 22 and 0.4 on December 30, demonstrating significantly higher accuracy than the previous two models.

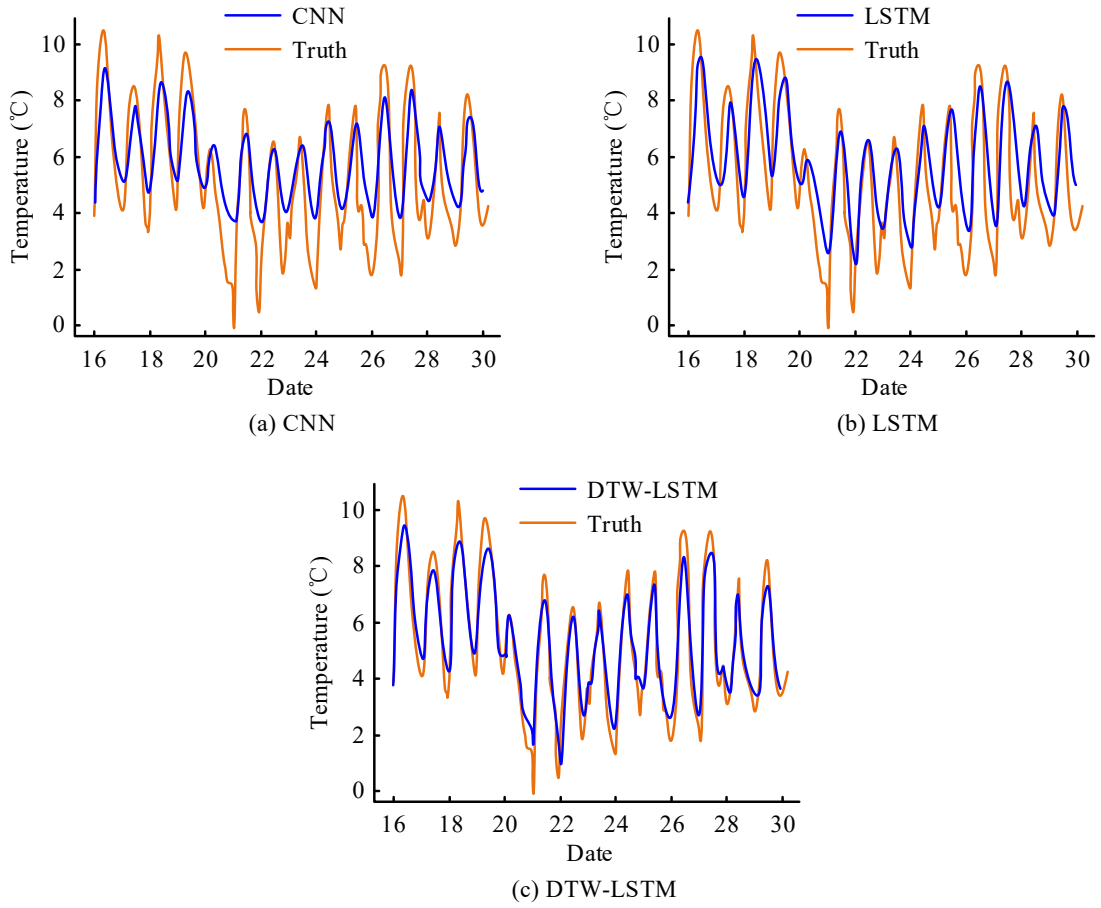

Fig. 5. Graphs of the predicted and true temperature values of different models

Fig. 6 compares the error performance of the DTW-LSTM, LSTM, and CNN models. In Fig. 6(a), the MAE of DTW-LSTM increases less than that of LSTM and CNN, consistently maintaining the lowest value. In Fig. 6(b), at 1h, the MAE of DTW-LSTM is 1.75. At time intervals such as 3h, 6h, and 12h, the MAE is significantly lower than that of the other two models. In Fig. 6(c), the MAE of DTW-LSTM increases gradually with time. At 12 hours, it remains the lowest among the three models, while the MAEs of LSTM and CNN consistently exceed that of DTW-LSTM. Overall, DTW-LSTM demonstrates superior error control and greater stability across all prediction durations at different time intervals.

Table 3 presents a comparison of the prediction performance between the DTW-LSTM fusion model and other models, covering four metrics: Mean Absolute Error (MAE), Root Mean Squared Error (RMSE), Mean Absolute Percentage Error (MAPE), and coefficient of determination (R^2). The Autoregressive Integrated Moving Average (ARIMA) model yields an MAE of 2.45, an RMSE of 3.12, an MAPE of 6.82%, and an R^2 of 0.76. The LSTM model reduces MAE to 1.23, with an RMSE of 1.87, MAPE of 3.56%, and R^2 of 0.89. The Transformer model achieves an MAE of 1.15, RMSE of 1.75, MAPE of 3.3%, and R^2 of 0.91. Meanwhile, DTW-LSTM demonstrates the best performance across all metrics: MAE of 0.92, RMSE of 1.35, and MAPE of 2.84%. Moreover, its R^2 value reaches 0.94, significantly outperforming models such as ARIMA, Support Vector Regression (SVR), and RF. This fully demonstrates the superior PA of the fusion model.

Fig. 7 presents the Anomaly Correlation Coefficient (ACC) prediction results for four key meteorological variables: Mean Temperature (MT), MaxT, MinT, and Dew Point Temperature (DPT). ACC measures the degree of anomalous matching between PV and AV of meteorological variables. Li et al. (2024) proposed a coupled prediction model ESMD-

EWT-SVD-LSTM consisting of Extreme Point Symmetric Mode Decomposition (ESMD), Empirical Wavelet Transform (EWT), Singular Value Decomposition (SVD), and LSTM. This study compared ESMD-EWT-SVD-LSTM with DTW-LSTM. In Fig. 7(a), the ACC of DTW-LSTM gradually decreases from 1.00, reaching 0.85 at 192 hours. The ACC of ESMD-EWT-SVD-LSTM declines more rapidly, reaching 0.75 at 192 hours. In Fig. 7(b), the DTW-LSTM achieves an ACC of 0.80 at 192 hours, while ESMD-EWT-SVD-LSTM drops to 0.65. In Fig. 7(c), the DTW-LSTM maintains an ACC of 0.42 at 192 hours, whereas ESMD-EWT-SVD-LSTM falls to only 0.22. In Fig. 7(d), the DTW-LSTM model exhibits a slower decline in ACC, reaching 0.35 at 192 hours, while ESMD-EWT-SVD-LSTM drops to 0.20. Overall, DTW-LSTM consistently achieves higher ACC than ESMD-EWT-SVD-LSTM in long-term forecasts for the four meteorological variables, exhibits slower decay over time, and delivers superior prediction accuracy.

Fig. 8 shows the RMSE prediction results for four key meteorological variables: MT, MaxT, MinT, and DPT. As the forecast time increases, the RMSE of both methods increases, but the RMSE of DTW-LSTM remains consistently lower than that of ESMD-EWT-SVD-LSTM. In Fig. 8(a), the RMSE of DTW-LSTM at 192 hours is 3.5, while that of ESMD-EWT-SVD-LSTM is 3.9. In Fig. 8(b), the RMSE of DTW-LSTM at 192 hours is 2.4, while that of ESMD-EWT-SVD-LSTM is 2.9. In Fig. 8(c), the DTW-LSTM achieves 1.3 at 192 hours, while ESMD-EWT-SVD-LSTM achieves 1.8. In Fig. 8(d), the DTW-LSTM achieves 1.5 at 192 hours, while ESMD-EWT-SVD-LSTM achieves 1.9. Overall, DTW-LSTM not only exhibits lower prediction errors across various meteorological variables but also shows a more gradual increase in error over time, indicating superior prediction accuracy and stability.

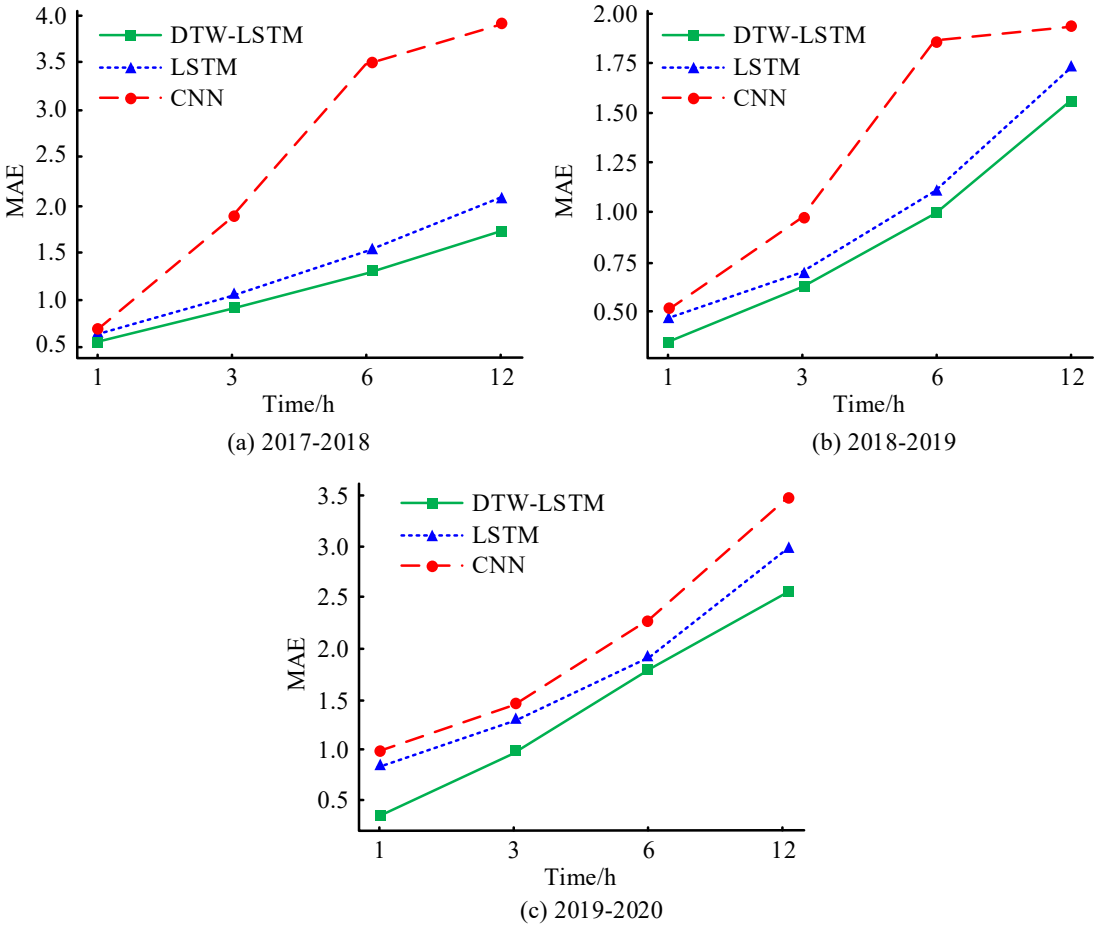

Fig. 6. Graph of the relationship between prediction duration and MA

Total precipitation serves as a key variable for measuring precipitation intensity and coverage, yet its significant spatio-temporal nonlinearity and sparsity pose substantial challenges for modeling and forecasting. Fig. 9 presents the predicted total precipitation. In Fig. 9(a), the ACC of the DTW-LSTM model gradually declines from 0.78 to 0.25 at 192 hours. The ACC of ESMD-EWT-SVD-LSTM decreases from 0.75 to 0.22 at 192 hours, while DTW-LSTM demonstrates overall superior ACC. In Fig. 9(b), the RMSE of DTW-LSTM gradually increases from 1.1 to 2.9 at 192 hours. The RMSE of ESMD-EWT-SVD-LSTM increases from 1.6 to 3.4 at 192 hours. DTW-LSTM consistently maintains a lower RMSE. It is precisely because DTW-LSTM can more effectively utilize historical meteorological variable data to capture the complex dynamic structure and multi-factor coupling relationships of total precipitation that it demonstrates superior performance in forecasting such highly uncertain variables.

Table 3. Comparison of prediction effects of DTW-LSTM fusion model

Model	MAE	RMSE	MAPE (%)	R^2
ARIMA	2.45	3.12	6.82	0.76
SVR	2.1	2.78	5.9	0.8
RF	1.85	2.4	5.2	0.84
XGBoost	1.75	2.25	4.95	0.86
BPNN	1.98	2.56	5.43	0.82
LSTM	1.23	1.87	3.56	0.89
Transformer	1.15	1.75	3.3	0.91
CNN-LSTM	1.08	1.6	3.05	0.92
DTW-LSTM (Ours)	0.92	1.35	2.84	0.94

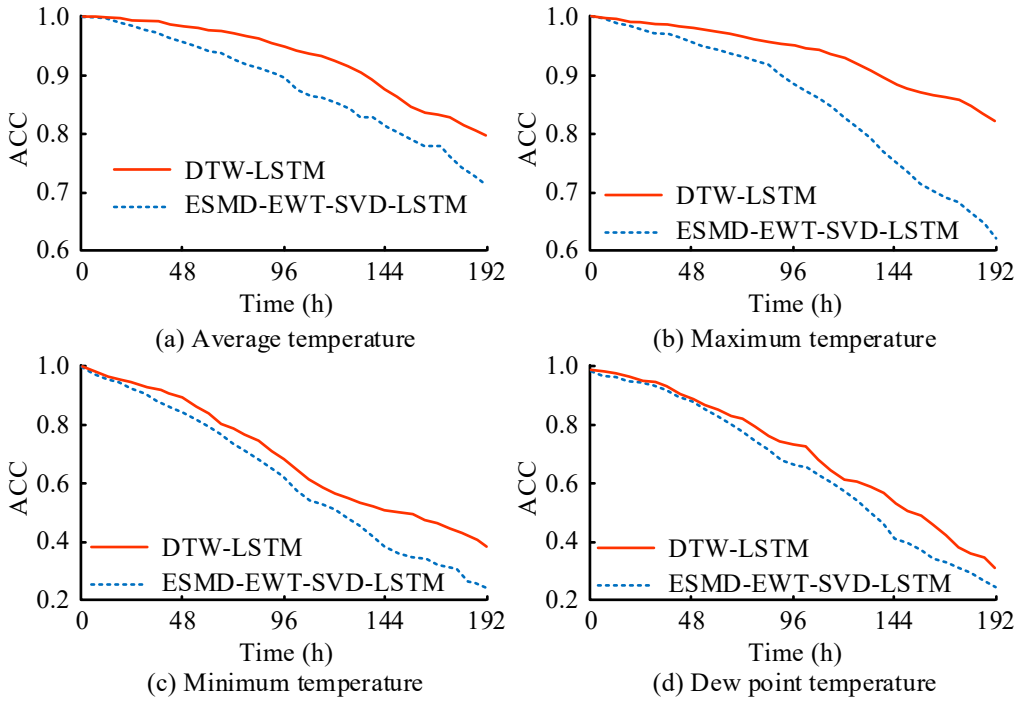

Fig. 7. The ACC prediction results of four important meteorological variables

3.2. Analysis of the Correlation Between Climate Suitability and Tourism Development

Fig. 10 shows the CCI changes in the Huangshan Scenic Area. In Fig. 10(a), the annual comprehensive climate comfort index of the Huangshan Scenic Area does not exhibit linear variation but rather fluctuates over time. This trend reflects the fluctuating adjustment characteristics of the scenic area's annual comprehensive climate comfort. Fig. 10(b) shows relatively significant changes in February, August, and October-November, which are closely correlated with air temperature: February increases from unsuitable to relatively unsuitable, October rises from relatively suitable to suitable, and November advances from relatively unsuitable to relatively suitable. Such improvements in comfort levels promote the development of tourism in scenic areas. Conversely, August declines from relatively suitable to relatively unsuitable, exerting a certain inhibitory effect on tourism activities. The comfort index for the remaining months changes relatively little, and the "M"-shaped pattern of climate comfort variation throughout the year gradually widens over time. Overall, during the 2010-2020 observation period, the annual comprehensive climate comfort index for Huangshan Scenic Area fluctuates upward, with a corresponding increase in the length of the tourist climate comfort period. This modification contributes to the sustained growth of the tourism sector in the picturesque region.

Table 4 presents the dimensionless processing results and correlation between the CCI and visitor numbers in Huangshan Scenic Area from 2010 to 2020. CCI values maintain a high level, reaching 0.92 in 2010, 1.02 in 2014, and 1.03 in 2019. Visitor numbers show a clear upward trend, increasing from 0.40 in 2010 to 0.88 in 2019 (slightly declining to 0.75 in 2020). The difference in dimensionless values steadily decreases, from 0.52 in 2010 to 0.13 in 2020, indicating

that the gap between CCI and visitor numbers is narrowing. Importantly, the correlation coefficient rises from 0.68 in 2010 to 0.83 in 2020, demonstrating that the influence of climate comfort on visitor numbers becomes increasingly significant over time.

Fig. 11 presents a heatmap of Pearson correlation coefficients between average temperature (1), MaxT (2), MinT (3), DPT (4), relative humidity (5), average wind speed (6), sea-level pressure (7), station-level pressure (8), and CCI (9). This clearly illustrates the association patterns between various meteorological elements and CCI. Temperature-related factors exhibit a highly positive correlation with CCI: The average temperature exhibits a correlation coefficient of 0.99 with CCI, while both maximum and MinTs show a correlation coefficient of 0.97 with CCI. The DPT correlates with CCI at 0.95. This indicates that air temperature and associated dew point conditions are core positive factors in enhancing climate suitability. Sea-level pressure exhibits a strong negative correlation with CCI (-0.86), indicating a significant inhibitory effect. Relative humidity (-0.24) and local barometric pressure (-0.27) show weak negative correlations with CCI, exerting minor influences. Average wind speed is nearly unrelated to CCI (-0.08), with negligible impact on suitability.

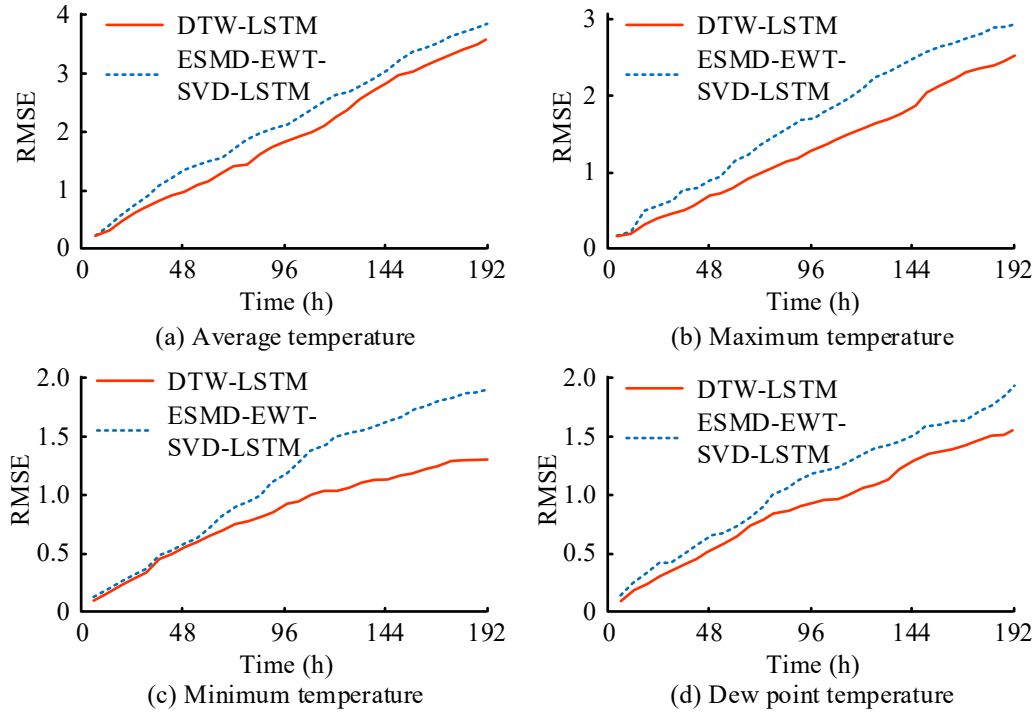

Fig. 8. The RMSE prediction results of four important meteorological variables

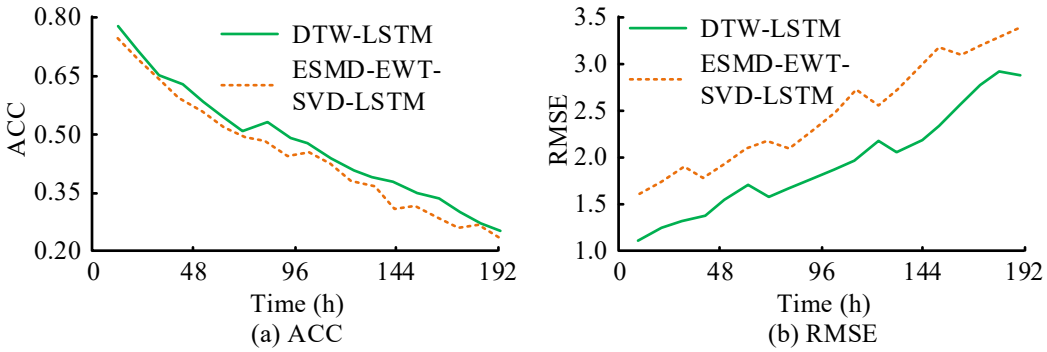

Fig. 9. Predicted results for total precipitation

4. Discussion

This study successfully developed a DTW-LSTM hybrid model and applied it to forecast climate suitability in scenic areas and analyze its connection with tourism growth. The experimental results confirmed the effectiveness and advantage of the proposed model, while the correlation analysis offered valuable quantitative evidence for understanding the complex link between climate and tourism. The DTW-LSTM fusion model showed notable improvements in prediction accuracy. Compared to the traditional LSTM model (MAE=1.23, RMSE=1.87), the DTW-LSTM model reduced MAE by 25.2% (to

0.92) and RMSE by 27.8% (to 1.35), with an R^2 value of 0.94. This suggests the model explains 94% of the variation in climate suitability. The improvements were especially evident in predicting extreme weather events and climate tipping points. In the late December 2018 forecast, the DTW-LSTM prediction curve closely matched actual values, with an average daily error of only 0.2-0.5. On days with large temperature swings, such as December 23, 27, and 30, errors reached nearly 0.9, but the model still surpassed the comparison model significantly. This shows the DTW algorithm helped the LSTM network by identifying "similar days" in historical data, providing more representative training samples. As a result, the LSTM network showed greater adaptability and stability when dealing with complex climate variation patterns.

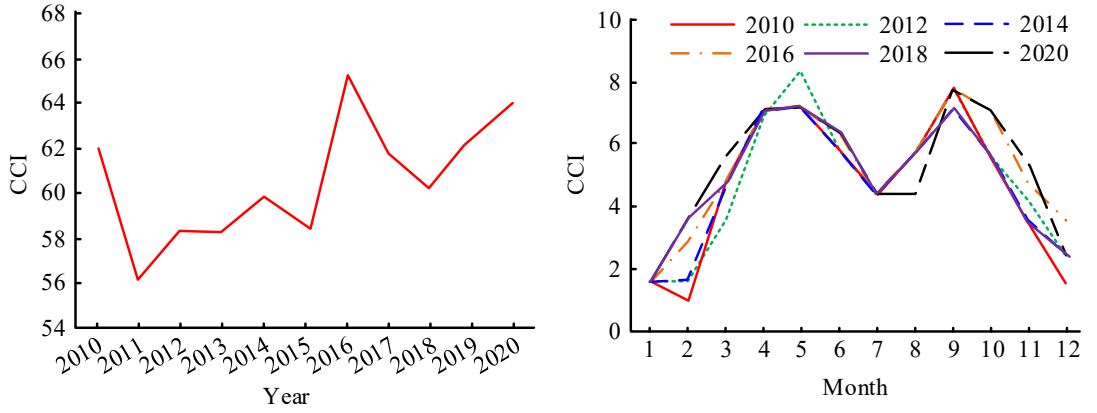

(a) Changes in CCI from 2010 to 2020 (b) Changes and evolution of CCI within the year

Fig. 10. Changes in CCI and comfort period in Huangshan Scenic Area

Table 4. Dimensionless processing results and correlation table of climate comfort index and number of tourists in Huangshan Scenic Area from 2010 to 2020

Year	Dimensionless processing value of CCI	The dimensionless processing value of the number of tourists in the scenic area	Dimensionless processing value difference sequence (absolute difference)	Correlation coefficient
2010	0.92	0.40	0.52	0.68
2011	0.95	0.45	0.50	0.69
2012	0.91	0.49	0.42	0.72
2013	0.98	0.54	0.44	0.71
2014	1.02	0.59	0.43	0.71
2015	0.97	0.65	0.32	0.75
2016	0.94	0.71	0.23	0.78
2017	1.01	0.76	0.25	0.77
2018	0.96	0.82	0.16	0.81
2019	1.03	0.88	0.15	0.82
2020	0.88	0.75	0.13	0.83

The DTW-LSTM model constructed by the researchers can not only predict the climate suitability of the scenic area with high accuracy but also provide a scientific decision-making basis for the scenic area management department. Firstly, scenic spots can dynamically adjust the ticket reservation system and entry policies based on the prediction results of climate suitability. One week before the suitable period, with a comfort index of ≥0.8, they can increase the number of online tickets and guide off-peak visits through price fluctuations. Before the unsuitable period, with a comfort index of ≤0.5, they can activate emergency plans to limit the number of group tourists and enhance the guidance of the flow of people. Second, human resources and facility allocation can be planned in advance based on predictions. For instance, ticket sales can be increased and off-peak visits guided during suitable weather periods, while flow control and diversion plans can be initiated during unsuitable weather periods. Third, differentiated tourism products and marketing activities can be designed based on predictions. During suitable periods, outdoor activities such as mountain climbing and sightseeing can be promoted, while during unsuitable periods, alternative products like cultural explanations can be launched. At the same time, climate comfort forecasts can be released through official platforms to help tourists plan their trips reasonably. Fourth, a climate risk emergency response mechanism should be established for extreme weather predictions, such as heavy rain and high temperatures. Medical points and spray cooling equipment should be deployed in advance during high

temperatures. During heavy precipitation, geological disaster monitoring should be strengthened, and dangerous sections of roads should be closed. Ecological adaptability projects, such as vegetation restoration and water resource management, can also be planned based on the trend of climate suitability changes to promote sustainable development. In conclusion, the model proposed by the research institute not only provides high-precision climate-suitability prediction tools for scenic spots but also establishes an effective closed loop from data prediction to management decision-making, helping scenic spots achieve refined, intelligent, and sustainable operations.

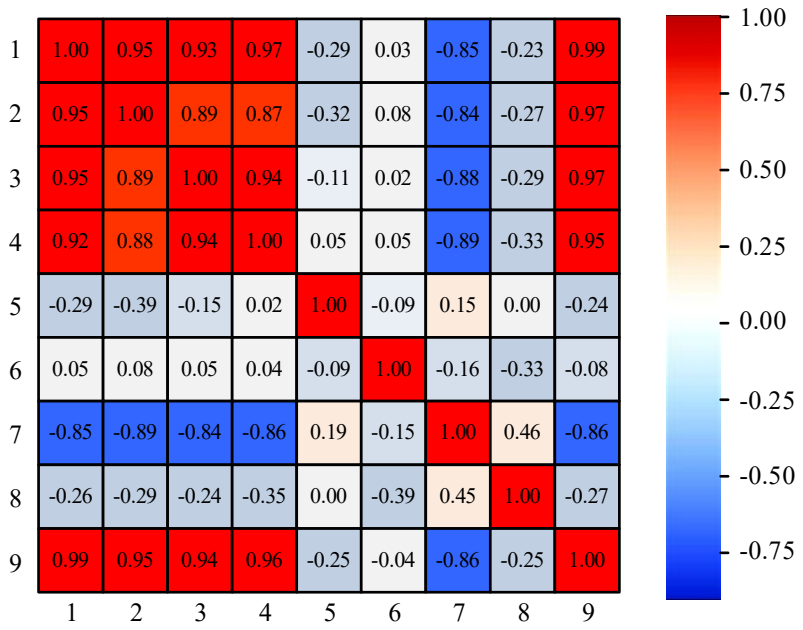

Fig. 11. Heat map of Pearson correlation coefficient of meteorological elements

Although this research achieves the expected results, it mainly focuses on climatic factors. While emphasizing their significant impact, tourist travel decisions are part of a complex, multi-faceted system. Factors like macroeconomic conditions, sudden public events, and marketing policies are not included in the model, which could reduce prediction accuracy in extreme situations. Furthermore, although this research case focuses on the Huangshan Scenic Area, as mentioned earlier, the model method has inherent portability. For instance, for seaside tourist destinations, the weights of "wind speed" and "sunshine" can be adjusted in the CCI calculation. For urban cultural tourism destinations, additional factors such as the "air quality index" that affect comfort can be included. Future research will focus on building an open framework that allows for flexible selection of features and adjustment of model parameters based on different types of tourist destinations. Through multi-case comparative studies, the model's adaptability and prediction accuracy will be systematically verified across different geographical, climatic, and cultural backgrounds.

5. Conclusion

This research developed a DTW-LSTM hybrid model to accurately forecast the timing of climate suitability in scenic areas and measured its correlation with tourism growth. In terms of prediction accuracy, the DTW-LSTM model significantly outperformed traditional and single DL models. Analyzing data from the Huangshan Scenic Area from 2010 to 2020, the model achieved an MAE of 0.92, an RMSE of 1.35, an MAPE of 2.84%, and an R^2 of 0.94. These results reflected MAE reductions of 62.5% and 25.2% compared to the ARIMA model and single LSTM model, respectively. In long-term forecasts, the model maintained excellent stability, reaching an average temperature accuracy of 0.85 at 192 hours, 0.1 points higher than the reference model. The total precipitation RMSE was 2.9, which was 0.5 lower than the reference, effectively capturing the nonlinear variability of climate data. This highlights the significant benefit of the DTW-LSTM fusion approach in modeling the nonlinear complexities and shape similarities within climate data. Regarding the correlation analysis, the CCI for Huangshan Scenic Area showed a fluctuating upward trend from 2010 to 2020. The correlation coefficient between CCI and visitor numbers increased from 0.68 to 0.83, indicating a stronger influence of climate suitability on tourism decisions. Additionally, the correlation coefficient between average temperature and CCI reached 0.99, establishing it as the primary positive factor impacting suitability. In conclusion, the DTW-LSTM model serves as an effective tool for predicting climate suitability. The correlation analysis results can provide quantitative support for managing visitor flow, designing tourism products, and fostering sustainable development in Huangshan Scenic Area.

Funding

The research is supported by Soft Science Project of Henan Provincial Department of Science and Technology in 2025. Research on the Internal Mechanism and Implementation Path of Empowering Henan's Cultural and Tourism Integration with New Quality Productivity for High Quality Development (Fund No. 252400410234).

Institutional Review Board Statement

Not applicable.

Declaration of Artificial Intelligence (AI) Tools

The author used DeepSeek solely for language editing and readability improvement. The author reviewed and verified all content and takes full responsibility for the accuracy and integrity of the manuscript

References

Alhindi, T. J., Alturkistani, O., Baek, J., and Jeong, M. K. (2025). Multi-Class Support Vector Data Description with Dynamic Time Warping Kernel for Monitoring Fires in Diverse Non-Fire Environments. *IEEE Sensors Journal,* 25(12), 21958-21970, DOI: 10.1109/JSEN.2025.3561725.

Basegmez, M. and Aydin, C. C. (2025). Climate change impact on green spaces planning in an urban area using a hybrid approach. *Environmental Science and Pollution Research*, 32(7), 4288-4312, DOI: 10.1007/s11356-025-35927-1.

Cao, H., Wu, Y., Bao, Y., Feng, X., Wan, S., and Qian, C. (2023). UTrans-Net: A model for short-term precipitation prediction. *Artificial Intelligence and Applications*, 1(2), 106-113, DOI: 10.47852/bonviewAIA2202337.

Cao, R. and Shang, P. (2024). Similarity measurement of symbolic sequence based on complexity estimate and dynamic time warping. *Nonlinear Dynamics*, 112(21), 19055-19070, DOI: 10.1007/s11071-024-10009-y.

Filipovska, M. and Mahmassani, H. S. (2023). Spatio-temporal characterization of stochastic dynamic transportation networks. *IEEE Transactions on Intelligent Transportation Systems*, 24(9), 9929-9939, DOI: 10.1109/TITS.2023.3276190.

Gebrehiwot, G. H., Bekitie, K. T., Abiko, F., and Seifu, W. (2024). Evaluation of CORDEX-Africa model data reliability and bias correction for climate change impact assessment: Upper Tekeze River Basin, Tigray (Ethiopia). *Green and Low-Carbon Economy,* 23(1), 1-12, DOI: 10.47852/bonviewGLCE42021893.

Gogen, E. and Guney, S. (2024). Machine learning-based weather prediction with radiosonde observations. *Journal of the Faculty of Engineering and Architecture of Gazi University*, 39(4), 2317-2328, DOI: 10.17341/gazimmfd.1163079.

Gong, G. Y., He, T., Chen, M., Wang, B., Nie, L., and Yin, Y. (2024). Spatio-temporal enhanced contrastive and contextual learning for weather forecasting. *IEEE Transactions on Knowledge and Data Engineering*, 36(8), 4260-4274, DOI: 10.1109/TKDE.2024.3362825.

Han, J., Liu, H., Zhu, H., and Xiong, H. (2023). Kill two birds with one stone: A multi-view multi-adversarial learning approach for joint air quality and weather prediction. *IEEE Transactions on Knowledge and Data Engineering*, 35(11), 11515-11528, DOI: 10.1109/TKDE.2023.3236423.

Huang, J., Li, J., Oh, J., and Kang, H. (2023). LSTM with spatiotemporal attention for IoT-based wireless sensor collected hydrological time-series forecasting. *International Journal of Machine Learning and Cybernetics*,14(10), 3337-3352, DOI: 10.1007/s13042-023-01836-3.

Kovács, A., Molnár, G., and Megyeri-Korotaj, O. A. (2025). Projected climate suitability for Hungarian tourism in the 21st century: application of the Holiday Climate Index and modified Tourism Climate Index. *International Journal of Biometeorology*, 69(6), 1429-1442, DOI: 10.1007/s00484-025-02901-y.

Li, F. (2024). Predicting Daily Tourist Flow in Scenic Areas Using LSTM and Big Data from Baidu Index. *Informatica*, 48(12), 33-40, DOI: 10.31449/inf.v48i12.6134.

Li, P., Liang, T., Cao, Y., Wang, X., Wu, X., and Lei, L. (2024). A novel Xi'an drum music generation method based on Bi-LSTM deep reinforcement learning. *Applied Intelligence*, 54(1), 80-94, DOI: 10.1007/s10489-023-05195-y.

Li, T., Chen, L., Sun, H., Hou, M., Lei, Y., and Zhi, K. (2025). Exploring diversity and time-aware recommendations: an LSTM-DNN model with novel bidirectional dynamic time warping algorithm. *Soft Computing*, 29(4), 2003-2013, DOI: 10.1007/s00500-025-10534-x.

Li, Z. and Zhang, X. (2024). A novel coupled model for monthly rainfall prediction based on ESMD-EWT-SVD-LSTM. *Water Resources Management*, 38(9), 3297-3312, DOI: 10.1007/s11269-024-03815-x.

Liu, S., Lu, N., Shang, Z., and Rathnayaka, R. M. (2024). A new grey relational analysis model of cross-sequences. *Grey systems: Theory and application*, 14(2), 299-317, DOI: 10.1108/GS-10-2023-0098.

Lopes, H. S., Remoaldo, P. C., Ribeiro, V., Martín-Vide, J., and Ribeiro, I. (2024). Clothing and Outdoor Thermal Comfort (OTC) in tourist environments: a case study from Porto (Portugal). *International Journal of Biometeorology*, 68(11), 2333-2355, DOI: 10.1007/s00484-024-02753-y.

Malinović-Milićević, S., Micić, J., Denda, S., Stanojević, G., Petrović, M. D., and Gajić, T. (2025). Intensification of thermal risk in a changing climate: findings from prominent tourism destinations along the eastern Adriatic coast. *International Journal of Biometeorology*, 69(1), 157-175, DOI: 10.1007/s00484-024-02800-8.

Pereira, S., Canhoto, P., and Salgado, R. (2024). Development and assessment of artificial neural network models for direct normal solar irradiance forecasting using operational numerical weather prediction data. *Energy and AI*, 15(1), 100314, DOI: 10.1016/j.egyai.2023.100314.

Quibus, L., Le Mire, V., Queyrel, J., Boulanger, X., Castanet, L., and Féral, L. (2022). Estimating Annual Temperate Rain Attenuation Distributions at 20/40 GHz With a High-Resolution Numerical Weather Prediction Model. *IEEE Antennas and Wireless Propagation Letters*, 22(3), 601-605, DOI: 10.1109/LAWP.2022.3219776.

Ridderstaat, J. (2023). Measuring hidden demand and price behavior from US outbound health tourism spending. *Tourism Economics*, 29(3), 759-787, DOI: 10.1177/13548166211067925.

Ruiz Reina, M. Á. (2025). Dynamic time warping: intertemporal clustering alignments for hotel tourism demand. *Computational Economics*, 65(5), 2625-2648, DOI: 10.1007/s10614-024-10656-8.

Sabarinath, A., Rajesh, A. N., Gunthe, S. S., and Kumar, T. V. L. (2023). Application of deep learning algorithms to correct bias in CMIP6 simulations of surface air temperature over the Indian monsoon core region. *International Journal of Climatology*, 43(16), 7496-7515, DOI: 10.1002/joc.8276.

Sato, R. and Fujimoto, Y. (2024). Rainfall Forecasting with LSTM by Combining Cloud Image Feature Extraction with CNN and Weather Information. *IEEJ Journal of Industry Applications*, 13(1), 24-33, DOI: 10.1541/ieejjia.23002926.

Shang, L., Wang, Y., Dong, X., Niu, P., and Ji, S. (2025). Sentiment Analysis of Scenic Users' Comment Using FastText and LSTM Model. *IEEJ Journal of Industry Applications*, 26(4), 471-478, DOI: 10.70003/160792642025072604006.

Sierra-Porta, D. (2025). Revised cross-correlation and time-lag between cosmic ray intensity and solar activity using Chatterjee's correlation coefficient. *Advances in Space Research*, 75(1), 1330-1342, DOI: 10.1016/j.asr.2024.10.065.

Singh, V. K., Sharma, K., and Sur, S. N. (2025). Acoustic scene classification using dynamic time warping technique based on short time Fourier transform and discrete wavelet transforms. *Circuits, Systems, and Signal Processing*, 44(3), 1887-1913, DOI: 10.1007/s00034-024-02895-9.

Wang, H., Hu, T., and Wu, H. (2023). Tourism demand with subtle seasonality: Recognition and forecasting. *Tourism Economics*, 29(7), 1865-1889, DOI: 10.1177/13548166231184300.

Xu, G., Ng, M. K., Ye, Y., Li, X., Song, G., Zhang, B., and Huang, Z. (2024). TLS-MWP: A tensor-based long-and short-range convolution for multiple weather prediction. *IEEE Transactions on Circuits and Systems for Video Technology*, 34(9), 8382-8397, DOI: 10.1109/TCSVT.2024.3379291.

Yan, X., Yao, L., and Zhou, D. (2024). Optimizing Tourism Service Quality in 5G Multimedia Environments Using Deep Learning: A Model-Based Empirical Study. Informatica, 48(22), 147-161, DOI: 10.31449/inf.v48i22.6806.

Zhang, C. and Zhou, W. (2025). Physics-aware dual-branch architectures for accurate weather predictions. *GeoInformatica*, 29(3), 491-516, DOI: 10.1007/s10707-025-00537-z.

Xiaojing Liu obtained her PhD in Economics from Henan University in 2016. Currently, she serves as a lecturer in the Tourism Management Department of the Business School, Xuchang University. She has conducted research projects on tourism, economics and sustainable tourism development and has published over 20 academic papers. Her research interests include tourism management, tourism geography, and tourism economics.